Quantitative characterization of metastatic disease in the spine. Part I. Semiautomated segmentation using atlas-based deformable registration and the level set method

M. Hardisty, L. Gordon, P. Agarwal, T. Skrinskas, and C. Whyne[a)]
Orthopaedic Biomechanics Laboratory, Sunnybrook Health Sciences Centre, 2075 Bayview Ave., Room UB-19, Toronto, Ontario, M4N 3M5, Canada

(Received 19 June 2006; revised 10 May 2007; accepted for publication 11 May 2007; published 5 July 2007)

Quantitative assessment of metastatic disease in bone is often considered immeasurable and, as such, patients with skeletal metastases are often excluded from clinical trials. In order to effectively quantify the impact of metastatic tumor involvement in the spine, accurate segmentation of the vertebra is required. Manual segmentation can be accurate but involves extensive and time-consuming user interaction. Potential solutions to automating segmentation of metastatically involved vertebrae are demons deformable image registration and level set methods. The purpose of this study was to develop a semiautomated method to accurately segment tumor-bearing vertebrae using the aforementioned techniques. By maintaining morphology of an atlas, the demons-level set composite algorithm was able to accurately differentiate between trans-cortical tumors and surrounding soft tissue of identical intensity. The algorithm successfully segmented both the vertebral body and trabecular centrum of tumor-involved and healthy vertebrae. This work validates our approach as equivalent in accuracy to an experienced user. © *2007 American Association of Physicists in Medicine*. [DOI: 10.1118/1.2746498]

Key words: spine, vertebrae, image registration, image segmentation, level set, atlas based registration, metastasis, breast cancer

I. INTRODUCTION

Spinal metastases occur in 90% of prostate, 75% of breast, 45% of lung, and 30% of renal terminal cancer patients.[1] The vertebral bodies are the most common site for metastatic involvement in the spine (80%) due to metastatic spread via the vertebral venous plexus[2] (Fig. 1). Existing standardized criteria for assessing treatment response in bone metastases are based on x-ray and skeletal scintigraphy information from the 1970s and are still used in clinical protocols to this day.[3] The ability of these modalities to accurately quantify metastatic involvement, tumor progression, or treatment response is limited, mostly arising from their two-dimensional nature. More recently, three-dimensional imaging modalities, computed tomography (CT) and magnetic resonance (MR) imaging have been used to assess metastatic involvement and evaluate clinical treatment response for patients with skeletal metastases. In the assessment of metastatically involved spines CT has advantages over MR in terms of its ability to quantify skeletal integrity. However, MR has an advantage over CT in its ability to assess spinal cord compression and tumourous infiltration. The focus of treating these patients is usually palliative and therefore CT is the imaging modality of choice as it gives superior information on biomechanical stability. For the most part, such assessments have been done in a relatively qualitative fashion; the CT and MR data are evaluated based on individual clinical experience rather than on accepted published criteria. Thus, accurate quantitative assessment of metastatic disease in bone is often considered immeasurable and, as such, patients with skeletal metastases are often excluded from clinical trials, which require definitive measurements of treatment effect.[3]

CT scanning provides the ability to visualize the extent and distribution of metastatic disease within the spine via bony destruction or sclerotic formation. In defining the extent of tumor invasion within a metastatically involved vertebrae, it is important to both determine the size of the tumor and its volume relative to the bone it has invaded. While clearly defined and contained lytic or sclerotic regions may be delineated through semiautomated seeded thresholding,[4] more complex mixed and multifocal lesions are more difficult to segment (Fig. 2).

In order to effectively quantify the impact of metastatic tumor involvement in the spine (volume, progression, type) accurate segmentation of the vertebra is required. In many vertebrae with lytic involvement, the tumor may breach the cortical shell of the vertebral body, in which case semiautomated techniques such as thresholding or region growing have difficulty defining the boundary between tumor tissue and the surrounding soft tissue. Manual segmentation can account for cortical breaches but involves extensive and time-consuming user interaction. As well, operator-associated dependence must be considered with respect to the repeatability of manually defined regions of interest (ROIs). The subjective and inconsistent nature of visually contouring ROIs from stacks of two-dimensional (2D) CT images viewed at nonstandardized grayscale mappings can hinder the accuracy and repeatability of the quantitative assessment.[5] As well, other factors such as the presence of

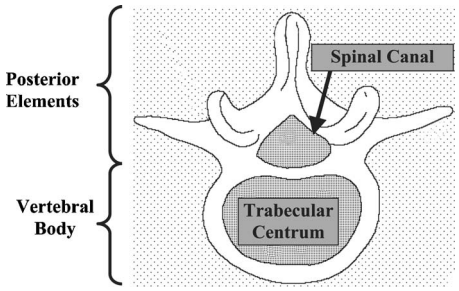

FIG. 1. Vertebral anatomy.

osteophytes appear as extensive areas of blastic activity that are adjacent to the vertebral bodies, which are in fact high density regions not related to the metastatic process. We propose that from within a defined and repeatable ROI, quantification of tumor involvement may be made through simple calculations of density or density distributions. If the ROI is not accurate and repeatable, however, such measurements will not reflect the true extent or response of spinal metastases.

A potential solution to automating segmentation of metastatically involved vertebrae, including those with cortical shell destruction, may be found in the application of demons deformable image registration[6] and the level set method.[7] Image registration refers to the spatial alignment of two images and can be used to segment structures by warping existing atlas segmentation to the geometry of a scan of interest. The level set method is a computational tool for tracking evolving interfaces based on curvature and intensity values.

Vertebral bodies have previously been the object of segmentation studies, however, sufficiently automated and accurate methods have not been presented in the literature. Kaminsky *et al.*[8] present many interesting tools to aid in the segmentation of vertebral bodies. These tools are quite versatile, however, they represent only an assistance to manual segmentation, consequently segmentations of vertebral bodies are quoted as taking between 29.7 and 102.8 min to complete. Hoad and Martel have presented a useful validated method to segment the lumbar spine.[9] The basis of the study was to develop a method to aid in computer-assisted surgery; as such the metrics used to assess the accuracy focused on the ability of the method to facilitate registration within surgery. The registration technique dealt with the poor contrast of bone when imaged with MR, which does not apply to the analysis of clinical CT scans. Kang *et al.*[10] and Mastmeyer *et al.*[11] both present methods of segmenting vertebral bodies, however, neither are validated against clinical scans nor are they designed to deal with the problematic cases that occur in tumour-involved vertebrae, such as breach of the cortical shell.

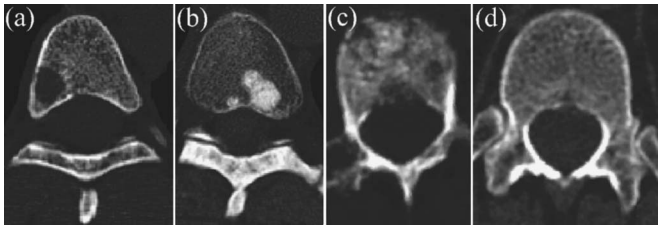

FIG. 2. Clinical CT slices of vertebral bodies representing different cases the algorithm will have to successfully segment: (a) a vertebrae with a distinct focal lytic lesion in the lower left vertebral body, (b) a vertebrae with a distinct focal blastic lesion in the lower right vertebral body, (c) a vertebrae with diffuse mixed involvement of the entire vertebral body, and (d) a healthy vertebral body.

Atlas segmentation has been used for the brain[12–14] and temporal tracking of the lungs, heart, and esophagus during a respiratory cycle.[15] General models of the organs of interest are deformed and molded to fit patient specific scans providing rapid and automated segmentations of these regions. The deformation algorithms involved in atlas registration have various approaches. Manual tagging of known landmarks to establish point correspondences with the atlas[12] has been used in the brain. More automated techniques, such as demons deformable registration,[6] are more robust and reduce inter/intrauser variability. Wu *et al.*[14] demonstrated the superiority of demons registration for the brain over more rigid routines such as automated image registration[16] and statistical parametric mapping.[17] Atlas registration is largely limited by the ability of the algorithm to identify unique contours and is best suited for regions that have little interpatient variability and appear distinct in the chosen scan. In this way, a single atlas can be used for many different specimens. Due to the consistent shape of vertebral bodies, atlas based segmentation may provide an accurate method for automated segmentation of healthy and pathologically involved vertebrae.

The level set method has been proven to be particularly powerful in segmenting cerebral vasculature in CT[18–20] and MR[21] angiography. The branching vasculature is well suited to level set evolution yielding automatic segmentations that have high inter/intrauser reproducibility.[18] The method has also been applied to segmentation of the liver,[22] left ventricle in ultrasonic cardiac images,[23] and cine-MR,[24] and the septum in echocardiography.[25] These applications demonstrate the versatility of the level set method across different parts of the body and imaging modalities. Furthermore, the inherent morphology of the vertebral body lends itself well to the application of the level set method.

The purpose of this study was to develop a semiautomated method to accurately segment tumor-bearing and healthy vertebral bodies. The focus of this article is the application of demons deformable registration with the level set method to accomplish a semiautomated method to define both the vertebral body and the trabecular centrum of the vertebral body. It was hypothesized that a multifaceted image analysis technique, combining atlas based demons deformable registration and the level set method, applied to three-dimensional (3D) CT reconstructions would yield accurate and repeatable segmentation of healthy and pathologically involved vertebral bodies. The establishment of such a technique will allow the quantification of tumor involvement as described in Part II[28] and ultimately enable accurate tracking of tumor progression or treatment effect in the metastatic spine.

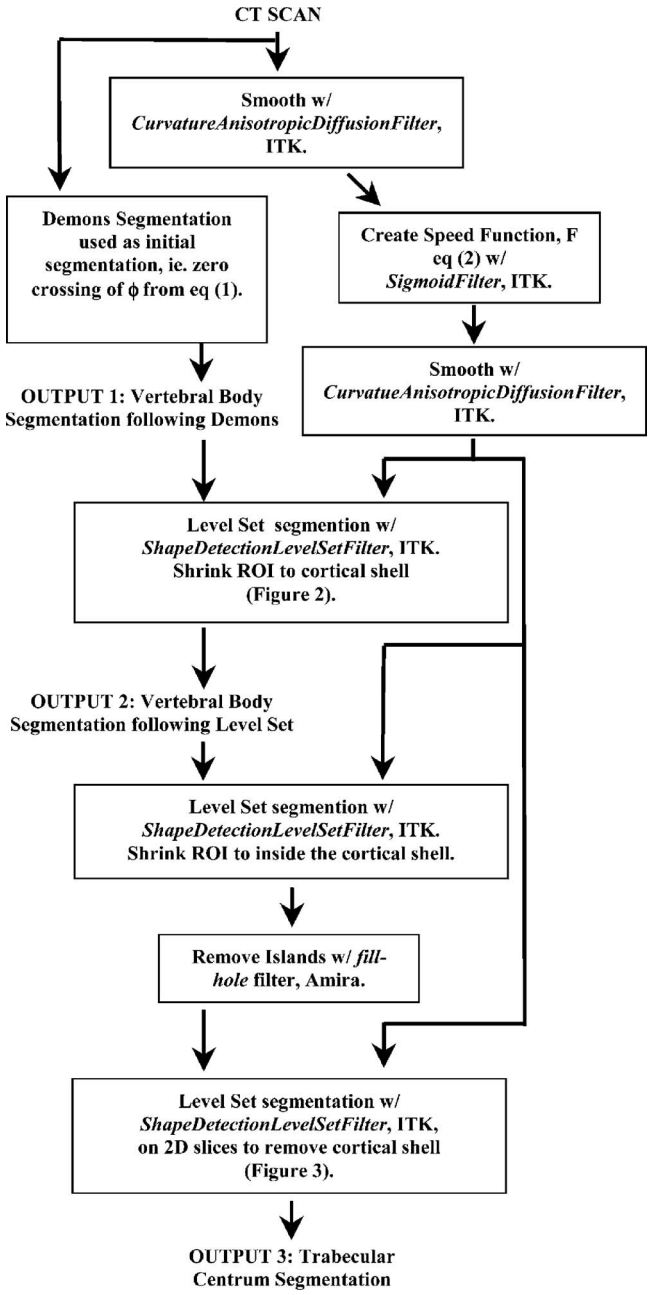

FIG. 3. Algorithm flow chart: A CT scan of a vertebra of interest is manipulated through various filtering schemes in order to obtain segmentations of the vertebral body and the trabecular centrum.

II. MATERIALS AND METHODS

Two separate methods of segmentation were combined to segment a vertebral body of interest from CT imaging data (Fig. 3). The first step in the segmentation process used demons deformable registration[6] of an atlas segmentation to a vertebral body of interest. The second step in the method refines the segmentation resulting from the first step using level set curvature evolution.[7] The segmentation algorithm was designed to identify two structures of interest, the trabecular centrum, and the greater vertebral body. The accurate identification of the trabecular centrum was the primary objective of this work because the overarching goal of the segmentation project was the definition of a region in which to quantify metastatic disease within vertebral bodies. Inclusion of the cortical shell in such a region can create problems for tumor quantification in mixed and blastic metastases as the cortical shell can display similar voxel intensity to blastic tumor tissue. As well, identification of the cortical shell is useful in its own right for biomechanical stability assessment and modeling purposes.

A. Atlas based demons deformable registration

An atlas of the healthy spine (T4-L5) was created, consisting of one patient scan for each individual vertebral body and a segmentation that defined the vertebral body within that particular scan for each level. Individual vertebrae scans were obtained by cropping larger scans obtained from six patients within the sample population. All patient scans were obtained from an ongoing breast cancer study (female, age average: 44, range: 32–64 years). All patients had some diseased vertebrae, thus, healthy vertebral levels from six patient scans were used to create the entire atlas. The atlas was developed using one segmentation from a single scan for each vertebral level. Scans were acquired on a GE Lightspeed Plus CT scanner using a standardized protocol at 120 kVp, with pixel sizes ranging from 0.35 to 0.47 mm in plane, 1.25 mm slice interval, and 2.5 mm slice thickness. Standard reconstructions, featuring enhanced contrast resolution, were used. The atlas segmentations were created by cropping and segmenting the vertebral body with a semiautomated threshold based approach (Amira 3.1.1, Mercury Computer Systems, Chelmsford, MA).

The segmentation begins with registration of an atlas from a corresponding spinal level to the vertebral body of interest. The procedure is performed in three steps. First, the atlas scan is spatially aligned with the scan of interest. The alignment is an initial manual step to ensure convergence of the algorithm. Second, an automated affine registration with 12 degrees of freedom, allowing for shearing, scaling, rotation, and translation is performed to initially register the two scans[26] (Amira). Finally, the two scans are deformably registered to a higher degree of accuracy using demons deformable registration. The resulting deformation field is then applied to the atlas segmentation yielding a semiautomated segmentation of the vertebral body of interest.

Before the implementation of the demons algorithm, all voxels in the atlas and patient scans with intensities below 150 Hounsfield units (HU) were set to 0 HU to prevent soft tissues from affecting the registration. The three-dimensional demons deformable registration was implemented in a multiresolution framework [Insight Toolkit (ITK), NLM, Bethesda, MO] with 35 iterations per resolution level with decreased downsampling in each progressive level to ensure a global best registration was found. The demons registration proceeds by optical flow, which tracks a deformation field that deforms the image locally by computing the difference between the images to be registered [Eq. (1)],

$$\mathbf{V}_t(X,t) = \frac{[I_2(X,t) - I_1(X)]\,\nabla I_1(X)}{[\nabla I_1(X)]^2 + [I_2(X,t) - I_1(X)]},$$
$$I_2(X,t) = I_2[X + \mathbf{V}(X,t)]. \tag{1}$$

In Eq. (1) an ideal vector field $[V(X,t)]$ is found that maps the moving image (I_2) onto fixed image (I_1). $V(X,t+1)$ is found by adding $V(X,t)$ to $V_t(X,t)$ until $V(X,t)$ suitably matches I_2 to I_1. The registration deforms the moving image in the direction of local normals of isointensity contours. After the completion of each resolution level, the deformation field is linearly interpolated to the resolution of the next finer level. Deformable registration begins on the coarsest image resolution level of the multiresolution pyramid with 8× downsampling in the transverse directions and 2× in the axial direction. Downsampled images were created by first convolving the image with a 3D Gaussian [σ =(amount of downsampling/2)^2, 32 pixel kernel], and then subsampling this smoothed image. At the second resolution level, registration continues with another 35 iterations at 2 × downsampling in the transverse directions and no downsampling in the axial direction. The last level to be completed is the finest and most computationally intensive level of the pyramid with no downsampling in any direction. Between each iteration, the deformation field was smoothed by convolution with a 3D Gaussian (deformation field: σ=2 voxels, 32 pixel kernel) the smoothing of the deformation field gives the deformation field a more elastic like quality by introducing a slight coupling between adjacent pixels, which improves convergence of the algorithm. The number of iterations, the number of pyramid levels, and amount of downsampling in the multiresolution pyramid was chosen to balance computation time with improvement in registration accuracy and robustness. The deformation field produced by demons is then applied to the atlas segmentation. An image warper, relying on nearest neighbor interpolation and back-projection from the output image domain to the input image domain is used to transform the segmentation of the atlas, producing a semiautomated segmentation of the metastatic vertebral body.

B. Level set method algorithm

The following level set algorithm is used to refine the demons segmentation of the vertebral body and to segment the inner trabecular centrum. The CT scan is smoothed using an anisotropic diffusion filter with a modified curvature diffusion equation to remove any noise that may interfere with segmentation. [Eq. (2)] (ITK CurvatureAnisotropicDiffusionImageFilter),

$$I_t(X,t) = |\nabla I(X,t)|\,\nabla \cdot e^{-|\nabla I|^2/2k^2}\frac{\nabla I(X,t)}{|\nabla I(X,t)|}. \tag{2}$$

This filter preserves edges and finer detailed structures but does not enhance them, representing a good trade off between standard anisotropic filters and Gaussian filters. The smoothing is controlled by the following parameters: a conductance term, k, that regulates the smoothing at edges, a time step, Δt which governs how much smoothing is done on each iteration and the number of iterations. Conductance is set to k=9 with Δt=0.00625 for five iterations in this first use of the filter.[27]

Segmentation of the image is then done using a level set filter. This filter solves a level set partial differential equation [Eq. (3a)] using finite differencing. The level set approach is to imbed the contour of interest in a higher dimensional function, ϕ. The contour is defined as the zero-level set of ϕ (ϕ=0),

$$\phi_t + F|\nabla\phi| = 0. \tag{3a}$$

F is the speed function

$$F = \frac{(\mu - \lambda K)}{1 + \exp(-(I-\alpha)/\beta)} \tag{3b}$$

and governs how quickly the contour flows to find the ideal segmentation. F is a sigmoid function (ITK SigmoidImageFilter) of the pixel intensities with β representing the pixel intensity range and α the center of the intensity range. K is the Gaussian curvature of the surface defined as [Eq. (3c)],

$$K = \nabla \cdot \frac{\nabla\phi}{|\nabla\phi|}. \tag{3c}$$

In Eq. (3b), I is the image intensity at a specific point. Equation (3b) controls the relative importance of pure contraction and a curvature-based evolution which are weighted by μ and λ, respectively. A higher μ will cause faster contraction, while a higher λ will cause the curve to remain smooth and more round. This method of segmentation proceeds by evolution of the surface via changing of ϕ from Eq. (3a).

The initial value of ϕ, also called the zero crossing of ϕ, is set based upon the previously discussed demons segmentation, where all pixels inside the contour are defined as −1, while all pixels outside the surface are defined as 1. The earlier described use of level set methods was done with the ITK ShapeDetectionLevelSetFilter.

The level set filter was applied in three distinct steps, first to refine the demons segmentation of the vertebral body, second to move the segmentation boundary to be within the cortical shell of the vertebral body, and third and finally to segment the trabecular centrum. To facilitate all steps of the segmentation the image is first smoothed using the curvature based anisotropic diffusion filter (Δt=0.00625, c=9, seven iterations). To refine the segmentation of the entire vertebral body the following parameters were set for the speed function: pixel intensity range, α, was set to 140 HU and the center of the intensity range, β, was set to −5 HU. This initial speed function causes quick contraction of the contour in soft tissue (low intensity values) and slow contraction of the contour in bony regions (high intensity). The level-set propagation term, μ, was set to 25 and the curvature term, λ, used to smooth out areas of high curvature was set to 40 to avoid the segmentation front from advancing into lytic tumors that have breached the cortical shell. The evolution was

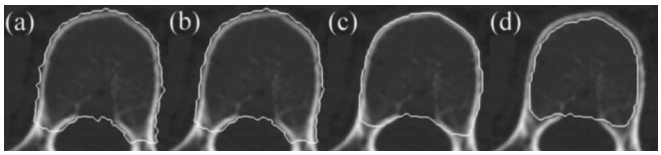

FIG. 4. Segmentation algorithm stages. 2D axial slices of computed tomography scans are depicted with a contour representing the current stage of segmentation: (a) initial demons segmentation of the exterior surface of the vertebral body, (b) the initial segmentation of the exterior surface of the vertebral body after refinement by level set, (c) the result of contracting the surface within the cortical shell by level set, and (d) the segmentation of the trabecular centrum after final processing with the level set filter.

allowed to proceed for 30 iterations to remove the gaps between the demons segmentation and the outer edge of the vertebral body (Fig. 4).

The following two steps are designed to segment the trabecular centrum with a starting point of the vertebral body segmented earlier. The first step simply allows the segmentation to come within the cortical shell; Parameters are set as $\mu=25$, $\lambda=50$, iterations=35, with the image intensity values set to constant. After contraction, a fill-hole filter (Amira) is applied to each axial scan slice to eliminate holes (size =2000 voxels) where the curve may have propagated into lytic tumor.

The final level-set segmentation was performed on each axial slice of the CT scan individually to ensure that the endplates are excluded from the trabecular centrum ROI. This necessity arises from the fact that flow with the influence of curvature will cause the contour to tend towards a spherical shape in three dimensions and will cause a curve in two dimensions to tend towards a circle. The vertebral body can be roughly approximated by a cylinder, thus using flow under curvature in two dimensions will favour the flow to the correct shape. The sigmoid speed function parameters were set to $\alpha=10$ and $\beta=350$, creating a speed function that will cause high speed motion through cortical bone (high image intensity) and slow motion through trabecular bone and soft tissue (middle and low image intensity). The level-set propagation parameters were set to $\mu=25$, $\lambda=70$, and 25 iterations; the high curvature weighting term helps to ensure the process does not exclude any blastic tumors connected to the cortical shell from the centrum ROI (Fig. 5).

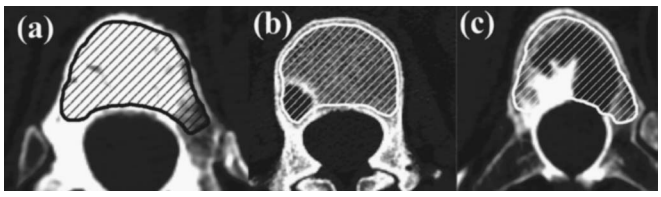

FIG. 5. Trabecular centrum segmentations. Depicted are 2D slices of sample segmentations for: (a) a highly blastic tumor adjacent to the cortical shell, (b) a well defined lytic lesion, and (c) a mixed lesion with cortical breach into the spinal canal. These three cases present particular challenges for manual and semiautomated segmentation techniques such as thresholding. Level set methods were able to define the trabecular centrum and demonstrate the functionality of the algorithm.

The algorithm after all segmentation was completed produced two useful contours, one defining the outside of the vertebral body and the other defining the outer boundary of the trabecular centrum (Fig. 4).

C. Algorithm training

All of the earlier mentioned parameters for segmentation were obtained empirically, using the earlier stated goal of the parameter as a starting point. The testing set consisted of specimens that representing healthy, blastic and mixed tumor cases, seven vertebral bodies in all were used during the development of the algorithm.

D. Algorithm testing

To test the algorithm, CT scans of tumor bearing vertebrae were collected using the same scanning parameters as previously mentioned. 20 vertebrae were collected from 13 patients with spinal metastases secondary to breast cancer. This set of vertebrae is distinct from the training set used to develop the algorithm, thus representing an unbiased sample of the data that would be collected in a clinical situation. Both healthy ($n=10$) and tumor-involved ($n=10$) vertebrae were segmented, lesions apparent in these vertebra included osteolytic ($n=4$), osteoblastic ($n=2$), and mixed lesions ($n=4$). Healthy vertebrae were obtained from the healthy vertebral levels within cancer patient scans. Lesions represented the spectrum of descriptions seen clinically including geographic, permeative, and moth-eaten appearances. Eighteen vertebrae with contained tumors and two vertebrae with breached cortical shells were analyzed. Vertebrae having osteophytes also present special challenges to automatic and manual segmentation; three vertebrae with osteophytes were included in the analysis. In total, six thoracic and 14 lumbar vertebral bodies, ranging in levels from T7 to L5 were segmented using the algorithm and compared to a gold standard manual segmentation performed by an experienced user.

Protocols for interpretation of the CT scans and the creation of the gold standard segmentations were made with consultation from radiologists and oncologists. The vertebral bodies (excluding the posterior elements) and the trabecular centrum were isolated using manual segmentation. The repeatability of the manual segmentation was assessed through inter- and intraobserver differences in which six scans were analyzed twice by a single user and once each by two additional users. A similar analysis was done to look at the repeatability of the semiautomated algorithm; six scans were analysed twice by a single user and once by an additional user.

The quality of the automatic segmentations were determined by calculating how many voxels were concurrently within both an automatic and a manual segmentation of the vertebral body and trabecular centrum. These values were then compared to the volume of the automatic and manual segmentations to determine the relative volume contained in both segmentations. An average of each relative volume was used to determine concurrency or quality of fit according to the following [Eq. (4)]:

TABLE I. Summary of segmentation results.

Mean+σ		N	Vertebralbody		Trabecular centrum
			Demons	Level set	Level set
Training set	Total	7	95.14%+2.41%	95.37%+2.26%	89.66%+3.69%
	Healthy	3	97.09%+1.24%	96.91%+1.35%	91.55%+2.46%
	Blastic	2	95.13%+0.91%	95.81%+0.46%	89.67%+2.64%
	Mixed	2	92.22%+1.73%	92.62%+1.9%	86.79%+4.26%
	Breached cortical shell	1	90.49%	90.72%	82.53%
Testing set	Total	20	95.07%+1.58%	95%+1.52%	89.28%+2.42%
	Healthy	10	95.21%+1.47%	95.23%+1.48%	89.08%+2.18%
	Blastic	2	96.02%+0.59%	95.4%+0.08%	89.51%+2.16%
	Lytic	4	95.2%+1.39%	95.35%+1.21%	91.44%+2.39%
	Mixed	4	94.11%+1.9%	93.9%+1.77%	87.53%+1.2%
	Breached cortical shell	2	93.54%+2.71%	93.66%+2.67%	90.05%+1.45%

$$\text{Concurrency}(\%) = \frac{1}{2}\left(\frac{\text{Vol}_{M\cap A}}{\text{Vol}_M} + \frac{\text{Vol}_{M\cap A}}{\text{Vol}_A}\right). \quad (4)$$

$\text{Vol}_{M\cap A}$ is the volume of the volumetric overlap of the manual and automatic volumes obtained, Vol_M is the volume of the manual segmentation, and Vol_A is the volume of the semi-automated algorithms segmentation,

To further quantify the extent of cortical shell removal by the level set steps, two-voxel intensity histograms were compared for each healthy vertebral body. The comparison was made between a manual segmentation of the vertebral body, including cortical shell and a segmentation representing the trabecular centrum determined using the level set method. A perfect trabecular centrum segmentation ought to result in complete removal of the cortical shell with 0% of the segmentation representing high intensity voxels (intensity values that are only found in the cortical shell in healthy vertebrae).

III. RESULTS

A. Manual inter/intrauser repeatability

The average intrauser concurrency of manually defined was 97.64%±1.32% for six segmentations that were repeated twice. The average interuser repeatability of manually defined segmentations for three individuals was 94.42%±1.99%.

B. Automatic inter/intrauser repeatability

The average intrauser concurrency of automatically defined segmentations for the demons definition of the vertebral body was 96.66%+1.34%, for the level set segmentation of the vertebral body was 96.23%+1.60%, and for the trabecular centrum was 95.74%±3.56 for five segmentations that were repeated twice. The average interuser concurrency of automatically defined segmentations for the demons definition of the vertebral body was 96.78%+1.52%, for the level set segmentation of the vertebral body was 97.43%+1.15%, and for the trabecular centrum was 94.86%±4.27% for five segmentations that were conducted by two different users.

C. Segmentation of the vertebral body

The deformable registration technique was able to successfully segment metastatically involved vertebrae with and without breach of the cortical shell. The initial demons segmentation was able to achieve a quality of the automatic segmentation of the vertebral body of 95.07%±1.58%. The level set revision of the initial demons segmentation of the vertebral body had a concurrency of 95.00%±1.52% (Table I). A continual decrease in accuracy was observed in moving superiorly in the spine from L5; this decrease was prominent above T7 (92.35%). A sample of the algorithms performance on top a CT slice is depicted in Fig. 4.

D. Segmentation of the trabecular centrum

In the ten healthy vertebral bodies, which include cortical shell, 21.1%±4.5% of the vertebral body segmentations were classified as high density, constituting cortical bone. After application of the level set algorithm, high density bone represented 3.6%±0.5% of the segmentation, indicating the cortical shell was not present within the trabecular centrum segmentation. Comparing the semiautomated segmentations of the trabecular centrum to manual segmentations yielded a concurrency rate of 89.28%±2.42%. For scans in which a lytic tumor had breached the cortical shell, the concurrency rate was 90.05%±1.45%. Scans containing a blastic tumor adjacent to the cortical shell exhibited a concurrency rate of 89.51%±2.16% (Table I). Sample segmentations on axial CT slices are given in Fig. 5.

The manual alignment stage takes about 10 s of user intervention. Average computation time for the algorithm in its entirety was 3 min 15 s±1 min 26 s over six timed runs on a 3 GHz Intel Pentium 4 with 1 GB random access memory.

IV. DISCUSSION

This study presents an algorithm that produces segmentations of both the vertebral body and the trabecular centrum, by combining two previously established segmentation methods. The first uses demons deformable registration to fit an atlas segmentation to a vertebra of interest. The second approach refines the resultant segmentation using level set curvature evolution to both refine the vertebral body segmentation and specifically define the trabecular centrum of the vertebral body. Both steps proved to be accurate in their respective goals.

Atlas-based segmentation is able to overcome many problems inherent to more conventional segmentation techniques such as region growing and thresholding. By maintaining the morphology of the atlas, the algorithm was able to accurately differentiate between trans-cortical tumors and surrounding soft tissue of identical intensity. Atlas-based segmentation is significantly faster than manual delineation of the volume or semiautomated threshold based methods that anecdotally take at least 10 min and up to 2 h to complete in complicated cases.

Most errors in the automatic demons segmentations were found near the upper and lower end plates. Future work is needed to improve the algorithm to better differentiate between disk tissue and bone and to account for large differences in shape (e.g., osteophytes) between the atlas and the patient scan which can cause significant inaccuracies in the segmentation. Elapsed time of the algorithm is dependent on the scan size. Smaller scans, and consequently smaller vertebra, were segmented more rapidly than larger scans. This is intuitive since the process runs on all voxels in the image, where more voxels require more computation time.

Level set shape detection methods are well suited for isolating the trabecular region in both healthy and metastatically involved vertebral bodies. By applying a large curvature term weighting, the ability of the curve to propagate into tumors and eliminate them from the ROI is limited. Furthermore, three vertebral levels in the analysis presented osteophytes that did not affect the accuracy of the results. The greatest errors in trabecular bone isolation occurred as a result of partial inclusion of the vertebral endplates; however, this is not a large concern as endplates contain few high intensity voxels, which might be incorrectly classified as blastic tumor tissue. Elapsed computation time was again related to image size and accounts for the high variance. The algorithm can successfully perform semiautomated segmentation of a vertebral body trabecular centrum to yield an appropriate ROI for quantitative assessment of metastatic disease and may be adapted to trabecular region segmentation in other bones exhibiting a rounded cross-sectional geometry.

Evaluating segmentation algorithms relative to a gold standard has been approached in many different ways in the literature and thus makes comparisons to our concurrency difficult. Furthermore, evaluations for different anatomies are not necessarily transferable to the spine. Nevertheless, reported accuracies for automated techniques, qualitative[15,25] or quantified[12,14,19,21,22] are always high or comparable to manual segmentations. Ganser *et al.*[12] reported surface matching accuracies of 4 mm in brain segmentations and Wu *et al.*[14] report that overlap ratios were 7.3% better for a demons algorithm compared to automated registration and statistical parametric mapping also for the brain. Level set segmentation has been applied to phantom data sets with 95% concurrency.[21] Cerebral vasculature diameters measured from level set segmentations had errors of 0.00 ± 0.23 mm and 0.00 ± 0.28 mm relative to phantom and manual measurements, respectively. To our knowledge, we have reported the first semiautomated segmentation technique for vertebral bodies and the trabecular centrum with results comparable to interuser variability using manual segmentation. Mastmeyer *et al.*[11] have reported segmentation of both the vertebral body and trabecular centrum, however, quantification of their algorithms performance was only assessed relative to a spine phantom and thus does not represent the complexities found in the clinical realm. Our approach has been shown to more rapidly yield equivalent segmentations to those performed manually by an experienced user and has spawned the development of tumor tracking scripts in our laboratory using the semiautomatically delineated ROIs.

With this established methodology, Part II[28] of this work uses the accurately defined ROIs to quantify tumor involvement. Where previously only qualitative description of disease progression was possible, quantifying tumor involvement will help increase the sensitivity of diagnoses, measure treatment effect, and perhaps aid in clinical decision making.

ACKNOWLEDGMENTS

The authors thank the Natural Science and Engineering Research Council of Canada and the Canadian Breast Cancer Research Alliance for their support. They would also like to thank radiologists Dr. Joel Rubenstein and Dr. Monique Christakis, radiation oncologist Dr Edward Chow, and medical oncologist Dr. Mark Clemons for their input. They would further like to thank Florence Wu for her assistance in the laboratory.

[a]Author to whom correspondence should be addressed. Electronic mail: cari.whyne@swri.ca

[1]D. A. Wong, V. L. Fornasier, and I. MacNab, "Spinal metastases: the obvious, the occult, and the impostors," Spine **15**, 1–4 (1990).
[2]J. K. Ratliff and P. R. Cooper, "Metastatic spine tumors," South Med. J. **97**, 246–253 (2004).
[3]T. Hamaoka, J. E. Madewell, D. A. Podoloff, G. N. Hortobagyi, and N. T. Ueno, "Bone imaging in metastatic breast cancer," J. Clin. Oncol. **22**, 2942–2953 (2004).
[4]D. L. Pham, C. Xu, and J. L. Prince, "Current methods in medical image segmentation," Annu. Rev. Biomed. Eng. **2**, 315–337 (2000).
[5]E. Chow, L. Holden, J. Rubenstein, M. Christakis, K. Sixel, M. Vidmar, J. Finkelstein, C. Hayter, A. Loblaw, R. Wong, E. Szumacher, and C. Danjoux, "Computer tomography (CT) evaluation of breast cancer patients with osteolytic bone metastases undergoing palliative radiotherapy—A feasibility study," Radiother. Oncol. **70**, 291–294 (2004).
[6]J.-P. Therion, "Image matching as a diffusion process: an analogy with Maxwell's demons," Med. Image Anal **2**, 243–260 (1998).
[7]S. Osher and J. A. Sethian, "Fronts propagating with curvature-dependent speed: Algorithms based on Hamilton–Jacobi formulation," J. Comput. Phys. **79**, 12–49 (1988).
[8]J. Kaminsky, P. Klinge, T. Rodt, M. Bokemeyer, W. Luedemann, and M. Samii, "Specially adapted interactive tools for an improved 3D-

segmentation of the spine," Comput. Med. Imaging Graph. **28**, 119–127 (2004).
[9]C. L. Hoad and A. L. Martel, "Segmentation of MR images for computer-assisted surgery of the lumbar spine," Phys. Med. Biol. **47**, 3503–3517 (2002).
[10]Y. Kang, K. Engelke, and W. A. Kalender, "A new accurate and precise 3-D segmentation method for skeletal structures in volumetric CT data," IEEE Trans. Med. Imaging **22**, 586–598 (2003).
[11]A. Mastmeyer, K. Engelke, C. Fuchs, and W. A. Kalender, "A hierarchical 3D segmentation method and the definition of vertebral body coordinate systems for QCT of the lumbar spine," Med. Image Anal **10**, 560–577 (2006).
[12]K. A. Ganser, H. Dickhaus, R. Metzner, and C. R. Wirtz, "A deformable digital brain atlas system according to Talairach and Tournoux," Med. Image Anal **8**, 3–22 (2004).
[13]B. C. Vemuri, J. Ye, Y. Chen, and C. M. Leonard, "Image registration via level-set motion: Application to atlas-based segmentation," Med. Image Anal **7**, 1–20 (2003).
[14]M. Wu, O. Carmichael, P. Lopez-Garcia, C. S. Carter, and H. J. Aizenstein, "Quantitative comparison of AIR, SPM and the fully deformable model for atlas-based segmentation of functional and structural MR images," Hum. Brain Mapp **27**, 747–754 (2006).
[15]D. Ragan, G. Starkschall, T. McNutt, M. Kaus, T. Guerrero, and C. W. Stevens, "Semiautomated four-dimensional computed tomography segmentation using deformable models," Med. Phys. **32**, 2254–2261 (2005).
[16]R. P. Woods, S. T. Grafton, J. D. Watson, N. L. Sicotte, and J. C. Mazziotta, "Automated image registration: II. Intersubject validation of linear and nonlinear models," J. Comput. Assist. Tomogr. **22**, 153–165 (1998).
[17]K. J. Friston, J. Ashburner, C. D. Frith, J.-B. Poline, J. D. Heather, and R. S. J. Frackowiak, "Spatial registration and normalization of images," Hum. Brain Mapp **2**, 165–189 (1995).
[18]R. Manniesing, B. K. Velthuis, M. S. van Leeuwen, I. C. van der Schaaf, P. J. van Laar, and W. J. Niessen, "Level set based cerebral vasculature segmentation and diameter quantification in CT angiography," Med. Image Anal **10**, 200–214 (2006).
[19]R. Manniesing and W. Niessen, "Local speed functions in level set based vessel segmentation," MICCAI **7**, 475–482 (2004).
[20]R. Manniesing, B. Velthuis, M. van Leeuwen, and W. Niessen, "Skeletonization for re-initialization in level set-based vascular tree segmentation," Proc. SPIE **5370**, 506–514 (2004).
[21]A. A. Farag, H. Hassan, R. Falk, and S. G. Hushek, "3D volume segmentation of MRA data sets using level sets," Acad. Radiol. **11**, 419–435 (2004).
[22]L. Hermoye, I. Laamari-Azjal, Z. Cao, L. Annet, J. Lerut, B. Dawant, and B. E. van Beers, "Liver segmentation in living liver transplant donors: comparison of semiautomatic and manual methods," Radiology **234**, 171–178 (2005).
[23]N. Paragios, "A level-set approach for shape-driven segmentation and tracking of the left ventricle," IEEE Trans. Med. Imaging **22**, 773–776 (2003).
[24]Y. Chenoune, E. Delechelle, E. Petit, T. Goissen, J. Garot, and A. Rahmouni, "Segmentation of cardiac cine-MR images and myocardial deformation assessment using level set methods," Comput. Med. Imaging Graph. **29**, 607–616 (2005).
[25]I. Dydenko, F. Jamal, O. Bernard, J. D'hooge, I. E. Magnin, and D. Friboulet, "A level set framework with a shape and motion prior for segmentation and region tracking in echocardiography," Med. Image Anal **10**, 162–177 (2006).
[26]L. Ibanez, W. Schroeder, L. Ng, and J. Cates, The ITK Software Guide, 2005.
[27]R. Whitaker and X. Xue, "Variable-conductance, level-set curvature for image denoising," Proc. IEEE International Conference on Image; 2001, pp. 142–145.
[28]C. M. Whyne, M. Hardisty, F. Wu, T. Skrinskas, M. Clemons, L. Gordon, P. S. Basran, "Quantitative characterization of metastatic disease in the spine. Part II. Histogram based analyses," Med. Phys. (submitted).